Sensors and Materials, Vol. 26, No. 8 (2014) 591–598
MYU Tokyo

S & M 1025

Fabrication and Characterization of d_{33} Mode $(1-x)Pb(Mg_{1/3}Nb_{2/3})O_{3-x}PbTiO_3$ (PMN-PT) Energy Harvester

Bin Yang*, Yanbo Zhu, Xingzhao Wang, Jingquan Liu and Chunsheng Yang

National Key Laboratory of Science and Technology on Micro/Nano Fabrication,
Institute of Micro and Nano Science and Technology,
Shanghai Jiao Tong University, Shanghai, 200240, China

(Received January 8, 2014; accepted June 12, 2014)

Key words: d_{33} mode, energy harvester, bonding and grinding, MEMS

In this manuscript, a d_{33} mode piezoelectric micro-electromechanical systems (MEMS) energy harvester integrated with silicon proof mass, which is made of composite cantilever beams from a silicon layer and a single crystal PMN-PT thick film, is proposed. The silicon mass is fabricated by the deep-reactive ion etching (DRIE) process to reduce the resonant frequency for a matching ambient source. A PMN-PT film of 15 μm thickness is realized by the hybrid process of wafer bonding and grinding. The experimental results show that this fabricated prototype can generate a maximum output voltage of 1.18 $V_{p\text{-}p}$ and corresponding power of 0.139 μW at the resonant frequency of 200 Hz and vibration acceleration of 2 g.

1. Introduction

With the rapid development of micro-electromechanical systems (MEMS) technology, microsensors and actuators for application in wireless sensor nodes and in the biomedical field have been developed. Because of the limitation of lifetime of batteries used for powering these devices, MEMS energy harvesters scavenging ambient vibration energy have been investigated by some researchers. There are three types of energy harvesting mechanisms to generate electricity from vibration, namely, electromagnetic,[1,2] electrostatic,[3,4] and piezoelectric[5,6] mechanisms. Mitcheson *et al*. compared the output performance limits of the three MEMS energy harvesting mechanisms.[7,8] Piezoelectric energy harvesters outperform electromagnetic harvesters at low frequency. They also generate high power density and are more suitable for microsystem applications.[9] The main research interest in piezoelectric energy harvesters is in the improvement of power generation. Shu and Lien studied the energy conversion efficiency of a piezoelectric energy harvester by an analytical model.[6] Ottman *et al*.

*Corresponding author: e-mail: binyang@sjtu.edu.cn

developed an adaptive electric circuit model to optimize the energy transfer from the piezoelectric element to the energy storage component.[10,11] Different piezoelectric materials have been developed in MEMS energy harvesters, such as PZT,[12] AlN,[13] ZnO,[14] PVDF,[15] and PMN-PT[16,17] single-crystal materials. Compared with other materials, the PMN-PT material exhibits outstanding piezoelectric properties that considerably surpass those of PZT ceramics by a factor of 4 to 5.[18] In addition to the optimization and selection of piezoelectric materials, some micromachining processes for thin and thick piezoelectric films have been proposed and developed, such as sol-gel,[5] aerosol,[19] and screen-printing[20] techniques. The thickness or piezoelectricity of the films formed by these methods is limited and very poor. A PZT thick film realized by bonding and lapping processes using Au as the intermediate layer has been used for vibration energy harvesters.[20] To reduce the micromachining cost, epoxy resins[21] and Cytop[22] are employed as a bonding layer for bulk PZT materials.

In this manuscript, a low-frequency vibration harvester based on a PMN-PT single crystal film, obtained using bonding and thinning processes, is proposed. The proposed device integrated with a silicon proof mass uses an interdigital electrode (IDE) pattern to maximize the efficiency of the energy conversion from environment vibration to electrical power. The fabrication of the MEMS-based PMN-PT energy harvester is demonstrated, and the output performance of this device is characterized and optimized.

2. Design and Fabrication

2.1 *Design of harvester*

Figure 1 shows the schematic of the d_{33} mode PMN-PT energy harvester. The composite cantilever is composted of a PMN-PT thick film, epoxy resin, SiO_2, and silicon supporting layers. The d_{33} mode of PMN-PT single-crystal materials is excited through an IDE, which can generate more energy and a larger tuning range than exhibited by the d_{31} mode structure.[23] In our previous works, the nickel mass was assembled on the cantilever tip manually.[24,25] This results in the mismatch of the location center of the cantilever and proof mass, causing the output performance and its conformance to be reduced. This process is not suitable for mass production in the future. In this study, a silicon proof mass is integrated at the tip of this composite cantilever.

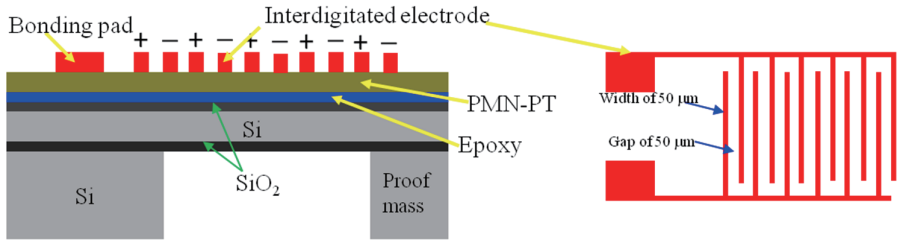

Fig. 1. (Color online) Schematic of d_{33} mode PMN-PT energy harvester.

The output average power for the load resistance can be expressed as[26]

$$P = \frac{RC_p^2(Nd_{33}c_2g/\varepsilon_{33})^2}{(RC_p\omega_0)^2(4\varsigma^2 + k_p^2) + RC_p 4\varsigma\omega_0(k_p^2/N) + 2\varsigma^2} \frac{\ddot{y}^2}{\omega_0^2}, \quad (1)$$

where N is the number of interdigital finger pairs, d_{33}, the piezoelectric constant, ε_{33}, the dielectric constant, c_2, the ratio of the stress of the piezoelectric layer to the vertical displacement of the proof mass, g, the gap between the IDEs, ς, the damping ratio, ω_0, the resonant frequency, k_p, the electromechanical coupling coefficient, R, the load resistor, and C_p, the total capacitance between the electrodes.

This equation shows that the piezoelectric constant d_{33} contributes to the high output power. Compared with other piezoelectric materials, the PMN-PT single crystal has higher piezoelectric constants.[27] Therefore, it can exhibit a better output performance.

The length and width of the composite cantilever are 4.8 and 1.2 mm, respectively. The width and gap of the IDE are 50 and 50 μm, respectively. The thicknesses of the thinned PMN-PT film, epoxy, silicon, and buried silicon dioxide are 15, 4, 7, and 2 μm, respectively. The proof mass helps to scavenge kinetic energy from low-frequency vibrations, hence allowing the generator to achieve better performance. The dimensions of the mass are 2000 × 1200 × 450 μm^3. The detailed design parameters are shown in Table 1.

2.2 *Fabrication of harvester*

The proposed MEMS piezoelectric energy harvester is fabricated using silicon-on-insulator (SOI) micromachining technology. The SOI wafer has a 5-μm-thick heavily doped silicon device layer, a 2-μm-thick buried oxide (BOX) layer and a 450-μm-thick silicon handle substrate. A 2-μm-thick silicon oxide layer was grown on both sides and deployed as an insulating layer and a hard mask for backside silicon etching. A 4-μm-

Table 1
Structural parameters of PMN-PT energy harvester.

	Description	Value
Cantilever	Length	4.8 mm
	Width	1.2 mm
	Silicon thickness	9 μm
	Epoxy thickness	4 μm
	PMN-PT thickness	15 μm
Silicon mass	Length	2 mm
	Width	1.2 mm
	Thickness	450 μm
Electrode	Length	3.65 mm
	Width	50 μm
	Gap	50 μm

thick epoxy resin was coated on a prepared wafer by screen printing, as shown in Fig. 2(a). The bulk PMN-PT of 400 μm thickness was bonded with the above prepared substrate [Fig. 2(b)]. The PMN-PT thickness was decreased to 15 μm by grinding and polishing [Fig. 2(c)]. The bonding optimization parameters have been detailed in our previous work.[24] The Cr/Au layer, as the IDE, is sputtered and patterned [Fig. 2(d)]. The bulk PMN-PT is patterned by mechanical dicing and the dicing thickness should be more than the total thickness of the device layer and buried oxide layer, as shown in Fig. 2(e). The backside oxide is patterned for the cantilever [Fig. 2(f)]. Finally, DRIE is carried out to remove the exposed silicon substrate stopping on the BOX layer.

The piezoelectric PMN-PT energy harvester array is fabricated, which includes cantilevers with different lengths and widths, as shown in Fig. 3(a). Figure 3(b) shows the backside view of the testing harvester. The integrated silicon proof mass can be clearly observed.

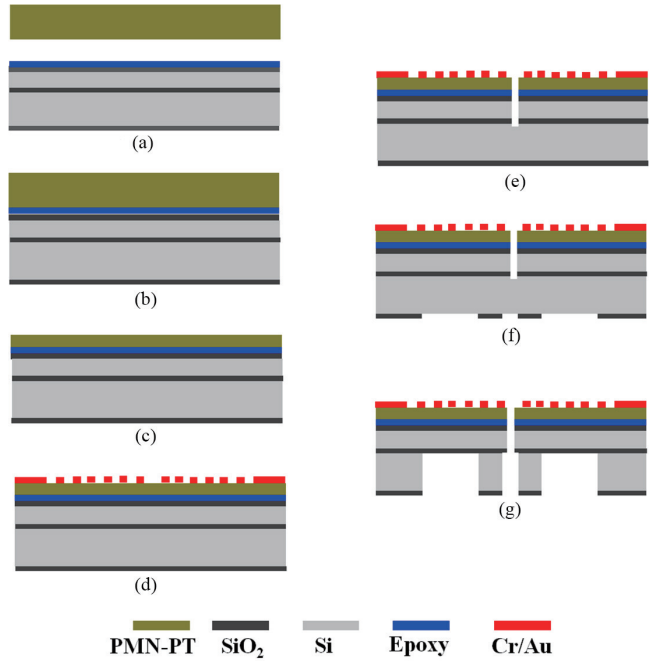

Fig. 2. (Color online) Fabrication process flow of PMN-PT energy harvester: (a) Deposited conductive epoxy resins by screen printing on SOI wafer; (b) Bonding bulk PMN-PT and SOI wafer; (c) Thinned down PMN-PT layer by mechanical grinding and polishing; (d) Deposited metal layer and pattern for IDE; (e) PMN-PT cantilever micromachining by dicing process; (f) Backside oxide patterning and etching by RIE; and (g) Backside silicon etching by DRIE, stopper at buried oxide layer.

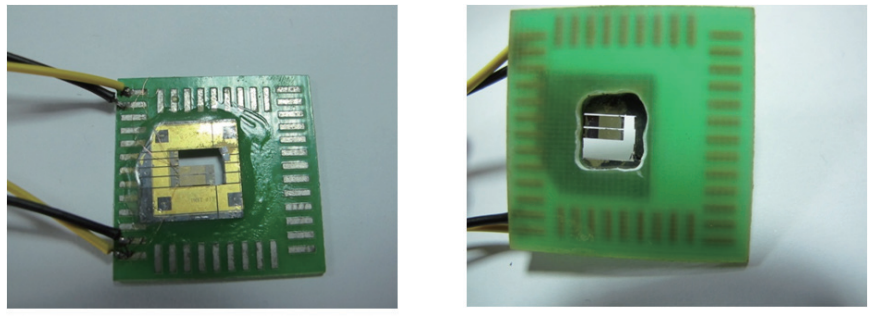

(a) (b)

Fig. 3. (Color online) Microfabricated piezoelectric d_{31} mode devices assembled with PCB: (a) Cantilever array energy harvester with wire bonding and (b) photograph of test prototype.

3. Testing and Characterization

3.1 *Testing platform*

The output performance of this prototype is evaluated using a vibration platform. It includes a function generator (Agilent 33220A), a power amplifier (SINOCERA YE 2706A), an accelerometer (SINOCERA YE5932A), an electromagnetic shaker (SINOCERA JZK-5) and an oscilloscope (Agilent 2000X). The device is attached to the shaker. The frequency and amplitude are tuned using the function generator and power amplifier, and the vibration acceleration is monitored using the accelerator attached to the shaker. The oscilloscope is used to measure the output voltage of this prototype under different vibration conditions. When this device is connected with load resistance, the output power delivered to this resistance can be calculated as

$$P = \left(\frac{V_{\mathrm{P-P}}/2\sqrt{2}}{R_{\mathrm{S}} + R_{\mathrm{L}}}\right)^2 R_{\mathrm{L}}, \tag{2}$$

where $V_{\mathrm{P\text{-}P}}$ is the loading output peak-peak voltage recorded by an oscilloscope, R_{S} is the internal resistance of the harvester, and R_{L} is the load resistance.

The maximum power is obtained when the internal resistance is equal to the load resistance, and it can be expressed as

$$P = (V_{\mathrm{P-P}}/2\sqrt{2})^2/R_{\mathrm{L}}. \tag{3}$$

3.2 *Characterization and discussion*

Before testing, the PMN-PT layer of the harvester was polarized by a DC electric field of 100 V on bonding pads for 2 h at room temperature. Figure 4 shows the output open-circuit voltages of the piezoelectric harvester from 197 to 211 Hz at different accelerations from 0.5 to 2 g. The measured maximum open-circuit output voltages excited from 0.5 to 2 g accelerations are 1.06, 1.63, 2.04, and 2.51 V at their corresponding resonant frequencies of 203, 202, 201, and 200 Hz. It is observed that the resonant frequency shifts towards lower frequencies with increasing acceleration, which results from the increasing damping ratio with acceleration owing to the nonlinearity of PZT under large stress. This low resonant frequency of the fabricated device can match one of the ambient vibration sources. For example, the acceleration and resonant frequency of a car engine compartment are 12 m/s^2 and 200 Hz, respectively.[28] The voltage increases by 54% from 1.06 to 1.63 V when the vibration acceleration increases from 0.5 to 1 g, while it only increases by 23% from 2.04 to 2.51 V when the vibration acceleration increases from 1.5 to 2 g. This is because of the nonlinear response of PZT, and the piezoelectric constant decreases with increasing stress when the acceleration amplitude increases.[29]

The closed-circuit output voltage under different load resistances is shown in Fig. 5(a). The loading voltage increases with increasing load resistance from 1 to 20 MΩ. The increase in the range of lower matching impedance is greater than that under the condition of higher impedance. Based on eq. (2), the corresponding output power is shown in Fig. 5(b). There is a peak value of output power under different vibration accelerations at the load resistance of 5 MΩ, which is named the optimal-matched resistance. The maximum output powers at 0.5, 1, 1.5, and 2 g are 0.024, 0.055, 0.09, and 0.139 μW, respectively. This result shows that the output power is low because the internal resistance of the prototype is very large, which will be improved through the optimization of the electrode gap in the future.

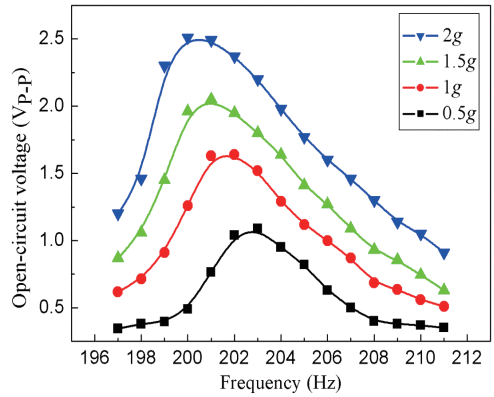

Fig. 4. (Color online) Output open-circuit voltage of PMN-PT energy harvester.

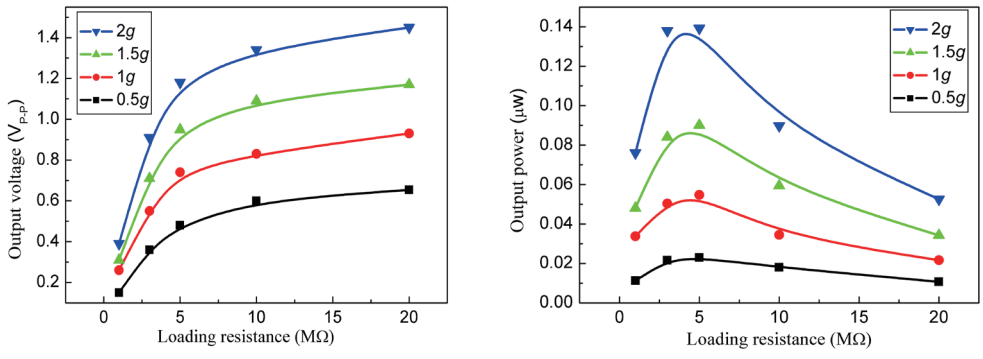

(a) (b)

Fig. 5. (Color online) (a) Output voltage under different load resistances and (b) output power under different load resistances.

4. Conclusions

A microfabrication process for a PMN-PT thick film energy harvester with an integrated silicon proof mass is developed. The key feature of the process is the realization of a film of uniform thickness with a high bonding force between the PMN-PT layer and the silicon substrate. The maximum open-circuit voltages at 0.5 and 2 g are 1.06 and 2.51 V at their corresponding resonant frequencies, respectively. Their corresponding maximum output powers are 0.024 and 0.139 μW, when the matched load resistance reaches 5 MΩ. In the future, we will improve the output power by optimizing the structure and electrode dimensions.

Acknowledgements

This work was supported in part by the National Natural Science Foundation of China under Grant Nos. 61204119, 51035005, and 61076107, 973 Program (2013CB329401), the Shanghai Pujiang Talent Plan Sponsorship (No. 13PJ1405100), Innovation Program of Shanghai Municipal Education Commission under Grant No. 14ZZ019, and the Science and Technology Department of Shanghai (No. 11JC1405700).

References

1 H. Liu, Y. Qian and C. Lee: Sens. Actuators, A **204** (2013) 37.
2 S. P. Beeby, R. N. Torah, M. J. Tudor, P. Glynne-Jones, T. O'Donnell, C. R. Saha and S. Roy: J. Micromech. Microeng. **17** (2007) 1257.
3 P. D. Mitcheson, P. Miao, B. H. Stark, E. M. Yeatman, A. S. Holmes and T. C. Green: Sens. Actuators, A **115** (2004) 523.
4 B. Yang, C. Lee, R. K. Kotlanka, J. Xie and S. P. Lim: J. Micromech. Microeng. **20** (2010) 065017.

5 H. Liu, C. J. Tay, C. G. Quan, T. Kobayashi and C. Lee: IEEE J. Microelectromech. Syst. **20** (2011) 1131.
6 Y. C. Shu and I. C. Lien: J. Micromech. Microeng. **16** (2006) 2429.
7 P. D. Mitcheson, E. M. Yeatman, G. K. Rao, A. S. Holmes and T. C. Green: Proc. IEEE **96** (2008) 1457.
8 P. D. Mitcheson, E. K. Reilly, T. Toh, P. K. Wright and E. M. Yeatman: J. Micromech. Microeng. **17** (2007) S211.
9 G. Poulin, E. Sarraute and F. Costa: Sens. Actuators, A **116** (2004) 461.
10 G. K. Ottman, H. F. Hofmann, A. C. Bhatt and G. A. Lesieutre: IEEE Trans. Power Electron. **17** (2002) 669.
11 G. K. Ottman, H. F. Hofmann and G. A. Lesieutre: IEEE Trans. Power Electron. **18** (2003) 696.
12 H. Liu, C. Lee, T. Kobayashi, C. J. Tay and C. Quan: Sens. Actuators, A **186** (2012) 242.
13 K. Karakaya, M. Renaud, M. Goedbloed and R. V. Schaijk: J. Micromech. Microeng. **18** (2008) 104012.
14 B. Yang, C. Lee, G. W. Ho, W. L. Ong, J. Liu and C. Yang: IEEE J. Microelectromech. Syst. **21** (2012) 776.
15 J. Fang, H. Niu, H. Wang, X. Wang and T. Lin: Energy Environ. Sci. **6** (2013) 2196.
16 A. Mathers, K. S. Mon and J. Yi: IEEE Sensors J. **9** (2009) 731.
17 K. Ren, Y. Liu, X. Geng, H. F. Hofmann and W. M. Zhang: IEEE Trans. Ultrason. Ferroelect. Freq. Contr. **53** (2006) 631.
18 I. A. Ivan, M. Rakotondrabe, J. Agnus, R. Bourquin, N. Chaillet, P. Lutz, J. C. Poncot, R. Duffait and O. Bauer: Rev. Adv. Mater. Sci. **24** (2010) 1.
19 B. S. Lee, S. C. Lin, W. J. Wu, X. Y. Wang, P. Z. Chang and C. K. Lee: J. Micromech. Microeng. **19** (2009) 065014.
20 K. Tanaka, T. Konishi, M. Ide and S. Sugiyama: J. Micromech. Microeng. **16** (2006) 815.
21 X. H. Xu and J. R. Chu: J. Micromech. Microeng. **18** (2008) 065001.
22 Z. H. Wang, J. M. Miao and C. W. Tan: Sens. Actuators, A **149** (2009) 277
23 R.K. Ryan, C. Mo and W.C. William: Proc. SPIE, 2009, 72880A1-9.
24 G. Tang, J. Liu, B. Yang, J. Luo, H. Liu, Y. Li, C. S. Yang, D. He, V. D. Dao, K. Tanaka and S. Sugiyama: J. Micromech. Microeng. **22** (2012) 065017.
25 G. Tang, J. Liu, B. Yang, J. Luo, H. S. Liu, Y. G. Li, C. S. Yang, V. D. Dao, K. Tanaka and S. Sugiyama: Electron. Lett. **48** (2012) 1.
26 J. C. Park, J. Y. Park and Y. P. Lee: IEEE J. Microelectromech. Syst. **19** (2010) 1215.
27 C. L. Sun, Q. F. Qin, F. Li and Q. M. Wang: J. Intell. Mater. Syst. Struct. **20** (2009) 559.
28 S. Roundy, P. K. Wright and J. Rabaey: Comput. Commun. **26** (2003) 1131.
29 D. Shen, J. H. Park, J. Ajitsaria, S. Y. Choe, H. C. W. III and D. J. Kim: J. Micromech. Microeng. 1**8** (2008) 055017.